The role of hot spot mix in the low-foot and high-foot implosions on the NIF

T. Ma, P. K. Patel, N. Izumi, P. T. Springer, M. H. Key, L. J. Atherton, M. A. Barrios, L. R. Benedetti, R. Bionta, E. Bond, D. K. Bradley, J. Caggiano, D. A. Callahan, D. T. Casey, P. M. Celliers, C. J. Cerjan, J. A. Church, D. S. Clark, E. L. Dewald, T. R. Dittrich, S. N. Dixit, T. Döppner, R. Dylla-Spears, D. H. Edgell, R. Epstein, J. Field, D. N. Fittinghoff, J. A. Frenje, M. Gatu Johnson, S. Glenn, S. H. Glenzer, G. Grim, N. Guler, S. W. Haan, B. A. Hammel, R. Hatarik, H. W. Herrmann, D. Hicks, D. E. Hinkel, L. F. Berzak Hopkins, W. W. Hsing, O. A. Hurricane, O. S. Jones, R. Kauffman, S. F. Khan, J. D. Kilkenny, J. L. Kline, B. Kozioziemski, A. Kritcher, G. A. Kyrala, O. L. Landen, J. D. Lindl, S. Le Pape, B. J. MacGowan, A. J. Mackinnon, A. G. MacPhee, N. B. Meezan, F. E. Merrill, J. D. Moody, E. I. Moses, S. R. Nagel, A. Nikroo, A. Pak, T. Parham, H.-S. Park, J. E. Ralph, S. P. Regan, B. A. Remington, H. F. Robey, M. D. Rosen, J. R. Rygg, J. S. Ross, J. D. Salmonson, J. Sater, D. Sayre, M. B. Schneider, D. Shaughnessy, H. Sio, B. K. Spears, V. Smalyuk, L. J. Suter, R. Tommasini, R. P. J. Town, P. L. Volegov, A. Wan, S. V. Weber, K. Widmann, C. H. Wilde, C. Yeamans, and M. J. Edwards

Citation: Physics of Plasmas **24**, 056311 (2017); doi: 10.1063/1.4983625

View online: http://dx.doi.org/10.1063/1.4983625

View Table of Contents: http://aip.scitation.org/toc/php/24/5

Published by the American Institute of Physics

The role of hot spot mix in the low-foot and high-foot implosions on the NIF

T. Ma,[1,a)] P. K. Patel,[1] N. Izumi,[1] P. T. Springer,[1] M. H. Key,[1] L. J. Atherton,[1] M. A. Barrios,[1] L. R. Benedetti,[1] R. Bionta,[1] E. Bond,[1] D. K. Bradley,[1] J. Caggiano,[1] D. A. Callahan,[1] D. T. Casey,[1] P. M. Celliers,[1] C. J. Cerjan,[1] J. A. Church,[1] D. S. Clark,[1] E. L. Dewald,[1] T. R. Dittrich,[1] S. N. Dixit,[1] T. Döppner,[1] R. Dylla-Spears,[1] D. H. Edgell,[2] R. Epstein,[2] J. Field,[1] D. N. Fittinghoff,[1] J. A. Frenje,[3] M. Gatu Johnson,[3] S. Glenn,[1] S. H. Glenzer,[4] G. Grim,[1] N. Guler,[5] S. W. Haan,[1] B. A. Hammel,[1] R. Hatarik,[1] H. W. Herrmann,[5] D. Hicks,[1] D. E. Hinkel,[1] L. F. Berzak Hopkins,[1] W. W. Hsing,[1] O. A. Hurricane,[1] O. S. Jones,[1] R. Kauffman,[1] S. F. Khan,[1] J. D. Kilkenny,[6] J. L. Kline,[5] B. Kozioziemski,[1] A. Kritcher,[1] G. A. Kyrala,[5] O. L. Landen,[1] J. D. Lindl,[1] S. Le Pape,[1] B. J. MacGowan,[1] A. J. Mackinnon,[4] A. G. MacPhee,[1] N. B. Meezan,[1] F. E. Merrill,[5] J. D. Moody,[1] E. I. Moses,[1] S. R. Nagel,[1] A. Nikroo,[1] A. Pak,[1] T. Parham,[1] H.-S. Park,[1] J. E. Ralph,[1] S. P. Regan,[2] B. A. Remington,[1] H. F. Robey,[1] M. D. Rosen,[1] J. R. Rygg,[2] J. S. Ross,[1] J. D. Salmonson,[1] J. Sater,[1] D. Sayre,[1] M. B. Schneider,[1] D. Shaughnessy,[1] H. Sio,[3] B. K. Spears,[1] V. Smalyuk,[1] L. J. Suter,[1] R. Tommasini,[1] R. P. J. Town,[1] P. L. Volegov,[5] A. Wan,[1] S. V. Weber,[1] K. Widmann,[1] C. H. Wilde,[5] C. Yeamans,[1] and M. J. Edwards[1]

[1]*Lawrence Livermore National Laboratory, Livermore, California 94550, USA*
[2]*Laboratory for Laser Energetics, University of Rochester, Rochester, New York 14623, USA*
[3]*Plasma Science and Fusion Center, Massachusetts Institute of Technology, Cambridge, Massachusetts 02139, USA*
[4]*SLAC National Accelerator Laboratory, Menlo Park, California 94025, USA*
[5]*Los Alamos National Laboratory, Los Alamos, New Mexico 87545, USA*
[6]*General Atomics, San Diego, California, USA*

(Received 14 December 2016; accepted 27 April 2017; published online 18 May 2017)

Hydrodynamic mix of the ablator into the DT fuel layer and hot spot can be a critical performance limitation in inertial confinement fusion implosions. This mix results in increased radiation loss, cooling of the hot spot, and reduced neutron yield. To quantify the level of mix, we have developed a simple model that infers the level of contamination using the ratio of the measured x-ray emission to the neutron yield. The principal source for the performance limitation of the "low-foot" class of implosions appears to have been mix. Lower convergence "high-foot" implosions are found to be less susceptible to mix, allowing velocities of >380 km/s to be achieved. *Published by AIP Publishing.*
[http://dx.doi.org/10.1063/1.4983625]

I. INTRODUCTION

Implosion studies carried out at the National Ignition Facility (NIF)[1] seek to demonstrate fusion ignition and burn via inertial confinement fusion (ICF). The approach requires the assembly of a thermonuclear fuel while maintaining a low overall adiabat. The resultant hot spot requires temperatures greater than 4–5 keV and areal densities sufficiently large ($\rho R > 0.3$ g/cm^2) to launch the burn wave, while the surrounding colder and denser DT shell (with a burn averaged total $\rho R \gtrsim 1.5$ g/cm^2) provides the extra burn and tamping to obtain high yield.[2,3]

To achieve these stagnated fuel conditions for ignition requires a high hot spot compression, high velocity, and symmetric implosion without hydrodynamic mix polluting the hot spot. In particular, heating from fusion reactions must surpass any cooling from conduction or x-ray losses. Lawson's criterion for fusion self-heating and ignition, or the $P\tau$, pressure × confinement time, scales as

$$P\tau \sim \epsilon^{1/2} \times \rho R \times vel, \quad (1)$$

where ϵ represents the hot spot coupling, ρR is the areal density of the hot spot, and *vel* is the velocity of the imploding shell, demonstrating the need for an efficient conversion of the kinetic energy of compression into thermal energy in the absence of mix to achieve the necessary hot spot coupling, high compression (>35) for the necessary ρR, and maximization of velocity (>350 km/s).

For a given drive, the maximum achievable compression is a function of fuel entropy and shell integrity. The growth of hydrodynamic instabilities due to surface imperfections or drive asymmetries degrades the uniformity of the implosion and can limit the distance an ablatively driven shell can be moved. There is thus an inherent tradeoff of implosion velocity, which is set by the mass ablation of the shell, and hydrodynamic mix, which increases as the shell becomes more susceptible to feedthrough of ablation front-driven Rayleigh-Taylor[4,5] instability growth. Higher Z material that penetrates into the hot spot will increase the radiative losses, quenching the burn and reducing the neutron yield.

Note: Paper NI2 1, Bull. Am. Phys. Soc. **61**, 222 (2016).
[a)]Invited speaker.

II. CRYOGENIC EXPERIMENTS AND DIAGNOSIS OF MIX

Mix is caused by hydrodynamic instabilities that grow at the various capsule interfaces or from features such as the fill tube, capsule support tent, or particulates on the capsule surface. The Rev. 5 capsule design[6] consists of a shell of CH plastic with an outside diameter of 2.26 mm and concentric layers of Si dopant. The total ablator thicknesses are varied, typically between 189 and 217 μm, and the Ge- or Si-doped layers are graded between 0% and 2%. The ablator encloses a spherical shell of DT fusion fuel. The DT ice layer of 69 μm-thickness and mass of 180 μg is kept solid by keeping the entire assembly at cryogenic temperature. This in turn surrounds a central sphere of DT vapor of 800 ng in equilibrium with the solid DT.

The capsule shell dopant of Ge or Si prevents inner ablator preheat by harder x-rays generated during peak drive,[7] allowing for a more favorable Atwood number to control the hydrodynamic instability at the ablator-ice interface.[8]

These capsules are imploded to ignition conditions by x-ray-driven ablation pressure generated by the interaction of the 192 beams of the NIF with the inside wall of the Au or depleted uranium (DU) hohlraum. X-ray heating of the shell exterior vaporizes it, creating expanding ablative flow and a pressure peak that drives the shell inward. Ablative acceleration, followed by deceleration by the return shock, is hydrodynamically unstable and can drive hydrodynamic instabilities. The dominant instability is the Rayleigh-Taylor (RT) instability arising at the ablation-front. Imperfections in the other surface of the capsule seed modulations that can grow, which in turn feed-through and seed perturbations on the interfaces of the capsule.

Any ablator material (which is primarily doped-CH) that mixes into the compressed fuel is heated and will emit strongly. This concurrently radiatively cools the hot spot, negatively impacting the performance of the fuel assembly and heating.

To date, we have utilized two methods of measuring mix in integrated implosions. The first is x-ray line spectroscopy of Ge-doped capsules.[9,10] Mix of the Ge-doped ablator into the hot spot will be heated to hot spot temperatures and emit characteristic line radiation. A time-integrated, 1D imaging spectrometer is used to record the x-ray spectra in the 6- to 16-keV range. This method has the advantage of quantifying the amount of mix derived from the Ge-doped layers and can determine the radial location the mix is derived from. However, a decision was made to replace the Ge dopant with Si in the autumn of 2011, which demonstrated improved radiation absorption and higher implosion velocity. Silicon, however, has no high energy x-ray lines capable of penetrating the high ρR ablator, so all of the radiated emission is continuum. So, the second method relies on continuum spectroscopy[11] and can be applied to any type of capsule and includes mix from all layers of the capsule. This paper will focus on mix derived by the continuum method.

III. THE MIX MODEL

The model quantifies the ablator mix into the hot spot by relying on the fact that the high-Z (Si-doped carbon) mixed into the hot spot radiates as Z_i^2 for free-free emission, and Z_i^4 for free-bound emission, increasing the radiated emission relative to a clean hot spot with only DT emission.

For DT implosions, the 14.1 MeV neutron yield from the fusion reaction $\mathrm{D}+\mathrm{T}\rightarrow{}^4\mathrm{He}\ (3.5\,\mathrm{MeV})+\mathrm{n}\ (14.1\,\mathrm{MeV})$ is given by

$$Y_{DT} = n_D n_T \langle \sigma_{DT} v(T_i) \rangle \mathrm{V}\, \tau_{burn}, \tag{2}$$

where Y_{DT} is the total 14.1 MeV neutron yield, n_D and n_T are the number densities of deuterium and tritium ions, respectively, $\langle \sigma_{DT} v(T_i) \rangle$ the DT reactivity cross-section at the ion temperature T_i, V the hot spot volume, and τ_{burn} the burn duration.

Using n_i the total ion density ($n_D + n_T$), with deuterium and tritium atomic fractions of f_D and f_T, respectively, we can rewrite Equation (2) using

$$n_D n_T = f_D f_T n_i^2 = f_D f_T \frac{A_v^2}{\bar{A}^2} \rho_{DT}^2 \tag{3}$$

such that

$$Y_{DT} = f_D f_T \frac{A_v^2}{\bar{A}^2} \rho_{DT}^2 \langle \sigma_{DT} v(T_i) \rangle \mathrm{V}\, \tau_{burn} \tag{4}$$

with A_v Avogadro's number, $\bar{A}$ the mean atomic mass, and ρ_{DT} the density.

The measured neutron yield is an average of individual measurements from the neutron activation diagnostics (NADs),[12] the magnetic recoil spectrometer,[13] and the neutron time-of-flight (NTOF) detectors.[14] Additionally, the ion temperature is also measured by the NTOFs. Hot spot volume is determined from 2D spatial x-ray imaging[15,16] measuring the spatial emission profiles along two orthogonal lines-of-sight, and the burn duration is measured by the Streaked Polar Instrumentation for Diagnosing Energetic Radiation (SPIDER).[17]

The x-ray emission from the hot spot after attenuation by the cold fuel and ablator shell looks like

$$X_\nu = 4\pi j_{DT} \times \left(1+\sum x_i Z_i\right)\left(1+\sum x_i \frac{j_i}{j_{DT}}\right) \times e^{-\tau_\nu^{shell}} \mathrm{V}\, \tau_{burn} \tag{5}$$

j_{DT} is the DT emissivity and is a function of the absorption coefficient $\alpha_{\nu,DT}$ and the blackbody function $B_\nu(T_e)$, and from fits to the Detailed Configuration Accounting (DCA) opacities[18] takes the form

$$j_{DT} = \alpha_{\nu,DT} B_\nu(T_e) = \frac{2.2}{\bar{A}^2} \rho_{DT}^2 \frac{1-e^{-h\nu/kT_e}}{(h\nu_{keV})^{0.33}}. \tag{6}$$

The $(1+\sum x_i Z_i)(1+\sum x_i \frac{j_i}{j_{DT}})$ term[3] in Eq. (5) is the enhancement factor that takes into account the multiple ion impurities with ionization Z, x_i is the atomic fraction of ion i in the DT, and $e^{-\tau_\nu^{shell}}$ (τ_ν^{shell} being the optical depth) is the absorption through the shell.

The emission coefficients for the other ion species (j_i) are also obtained from fits to the DCA model and have the

form of the j_{DT} equation. For a DT plasma, the emitted radiation is predominately free-free emission, but for CH or Si, both free-free and free-bound contributions are important. Fig. 1 shows the emissivity of a Si, CH, and DT plasma at conditions of 100 Gbar pressure and T_e of 2.0 keV. The CH and Si emissions are several orders of magnitude greater than the DT emissivity, demonstrating why using the x-ray continuum brightnesses can be used as a sensitive measurement of the number of emitters.

Two diagnostics measure the continuum emission from the hot spot: the Ross Pair Imager and South Pole Bang Time (SPBT). The Ross Pair diagnostic[15,16] employs differential filtering[19] to provide time-integrated, absolute x-ray self-emission images of the imploded core in five energy channels starting at 6 keV and above along the equatorial ($\phi = 90°$, $\theta = 78°$) and north polar ($\phi = 0°$, $\theta = 0°$) directions. Each of the channels of the Ross has overlapping spectral sensitivities (overlaps in bandwidth), so by simultaneously iterating the response of all five filters for the emission ($B_\nu \kappa_\nu$) of the hot spot × the absolute response of the channel, including the image plate (the recording medium) response and the filter transmission, a best fit can be found by χ^2 minimization for the emitted spectrum from the hot spot. In particular, as the radiation emitted by the hot spot in the 6–15 keV x-ray region is highly sensitive to absorption by the compressed shell, fitting the transmitted spectrum to the measured signal through each Ross filter also determines the optical thickness of the shell.

For a given shot, the full set of energies as measured through each channel of the Ross filter diagnostic can typically be fit to better than 5%. This provides the full unattenuated absolute x-ray spectrum from the hot spot with error bars of ∼30% and a detection threshold of CH(Si) mix mass of ∼100 ng. Shell attenuations calculated in this manner are also in agreement with post-shot Hydra simulations.[20]

The SPBT diagnostic[21,22] provides an additional measurement of the x-ray emission. SPBT views the implosion through the lower laser entrance hole of the hohlraum, uses a highly oriented pyrolytic graphite (HOPG) crystal to capture the emission from the hot spot within a narrow x-ray band around 10.85 keV, and records onto a PCD detector. When corrected for shell attenuation (by using the optical depth derived from the Ross Pairs), the SPBT gives an absolute measurement of the x-ray brightness.

The ratio of the x-ray to neutron yield is then independent of the hot spot density, volume, and burn width and scales only with temperature, shell attenuation, and mix fraction

$$\frac{X_\nu}{Y_{DT}} = \frac{4\pi}{f_D f_T A_v^2 \langle \sigma_{DT} v(T_i) \rangle} \frac{e^{-h\nu/kT}}{(h\nu)^{0.33}} \times \left(1 + \sum x_i Z_i\right)\left(1 + \sum x_i \frac{j_i}{j_{DT}}\right) \times e^{-\tau_\nu^{shell}}. \quad (7)$$

This ratio has only a slowly varying dependence on temperature—see Fig. 2 for the ratio as a function of ion temperature at an $h\nu = 10.85$ keV, so is relatively insensitive to uncertainties in the measured hot spot temperature.

The simplifying assumptions underlying Eq.(7) are that the same hot spot consistently produces neutrons and x-rays, the neutron and x-ray burn durations are the same, and $T_e = T_i$ locally. Neutron and x-ray sizes are measured on each shot by the Neutron Imaging System (NIS)[23] for primary 13–17 MeV neutron shape and gated[24] and time-integrated[15,16] x-ray imagers for broadband >6 keV x-ray emission shape. Images from both represent the hot spot profile and, when comparing equatorial line of sights from both types of images, are typically found to agree to within ∼10%. With respect to the hot spot temperature, recent work by Gatu *et al.*[25] indicates that fluid motion variations can contribute to an overly high inferred apparent ion temperature in the case of certain high yield, high temperature shots. Recent electron temperatures measured using high energy continuum spectroscopy[26] have been shown to be as much as several hundred eV below the inferred ion temperature. However, because accurate electron temperatures (T_e) were not easily derived for most of the shots discussed in this paper, for consistency, the ion temperatures (T_{ion}) are used across this set of shots in this analysis. Per Fig. 2, above T = 2.5 keV, substituting the electron temperature for the ion temperature would result in a higher x-ray to neutron yield ratio for a clean hot spot and thus decreased levels of estimated mix.

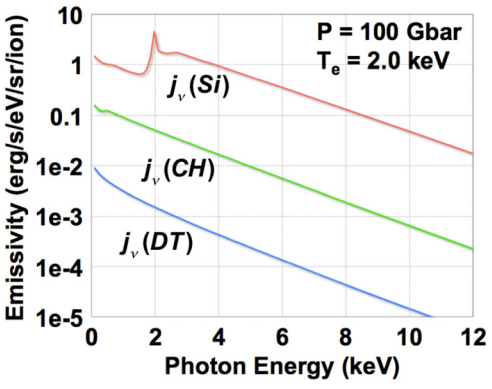

FIG. 1. Emissivity of a Si, CH, or DT plasma as a function of photon energy at a plasma pressure of 100 Gbar and electron temperature of 2.0 keV, from the DCA model.

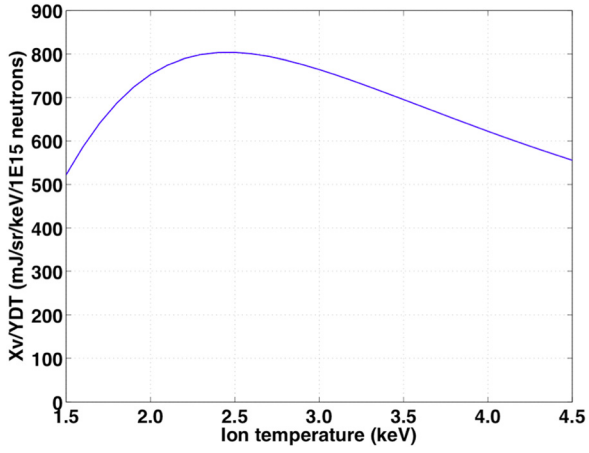

FIG. 2. X-ray to neutron ratio for clean DT at an $h\nu = 10.85$ keV.

Likewise, the temporal profiles of the neutron and x-ray emission typically agree to within ~20% (~40 ps). The neutron burn width is measured by the Gamma Reaction History (GRH) diagnostic with ~40 ps resolution.[27] The x-ray burn width is measured simultaneously by several diagnostics including two gated x-ray detectors (~30 ps resolution) and the SPIDER x-ray streak camera (<20 ps resolution). Simulations also indicate that no significant measurable difference in burn width between x-rays and neutrons is expected at the conditions of our present implosions.

A 1D isobaric model with radial-dependent density and temperature profiles is then applied to account for the radial weighting of x-rays and neutrons. This model assumes that the hot spot and surrounding fuel are in pressure equilibrium, with the temperature profile given as

$$T(r) = T_0\left[1 - \left(\frac{r}{r_0}\right)^2\right]^{0.331}; \tag{8}$$

and the density profile given as

$$\rho(r) = \frac{A}{(1+Z)A_v}\frac{P}{kT(r)}, \tag{9}$$

as described in Springer *et al.*[48] and illustrated in Fig. 3. Such a model is consistent with a 3D representation of the capsule density and temperature profiles at stagnation and has been validated by comparing results with 1D and 2D post-shot radiation-hydrodynamic simulations[30] and has produced semi-quantitative (10%–20%) agreement.

In this model, we assume that the electron temperature and ion temperature are locally equivalent, but account for T_i differing from the NTOF Brysk temperature by calculating the neutron spectrum and corresponding Brysk width. The model is fit to the measured yield, ion temperature, hot spot size, and burnwidth, to calculate the $T(r)$, $\rho(r)$, and pressure. This then allows us to account for the difference in radial weighting of x-rays and neutrons. This, however, is found to be a relatively small affect, as both neutrons and x-rays depend on the square of the density, and their yields as a function of temperature are found to vary slowly, as was shown in Fig. 2.

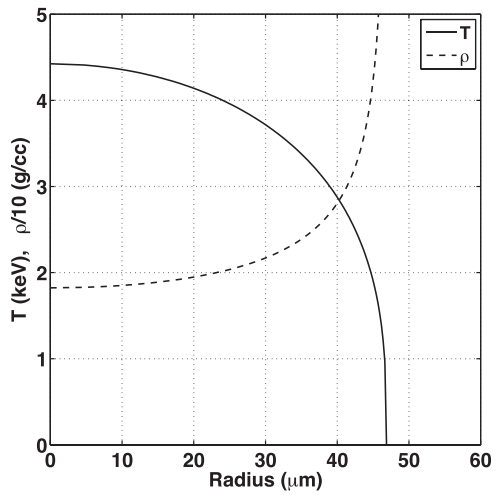

FIG. 3. The 1D isobaric model provides a radial-dependent density and temperature profile.

The ablator mix does not have to be uniformly distributed—to first order, the radiated emission is proportional to the total number of CH or CH(Si) ions, not the local ion density. This model directly calculates energy lost from the hot spot by radiation—this is the most relevant metric in terms of implosion performance or yield, and this enhancement is thus relatively robust to 2D and 3D effects for the reasons described above. In converting to a value for the nanograms of mix mass, then we make the assumption that the ablator composing the mix is from the most heavily doped layer. This is corroborated by 3D Hydra simulations by Clark *et al.*[28] In this case, we then also assume that the mix is atomically and homogeneously mixed into the hot spot and heated to the same hot spot temperatures. However, the calculation is valid to a good degree even if the CH(Si) is strongly localized, provided that the isobaric pressure and temperature equilibrium conditions are maintained in the hot spot volume. We can see this as follows: the x-ray emissivity of the CH(Si) mix is proportional to $n_e \times n_i$, the electron and ion number densities, respectively. For the case of uniform mix, the emissivity is proportional to $n_e \times n_i$ times the total hot spot volume, V. For a case where the same mix mass is confined to a fraction of the hot spot volume fV, the corresponding CH(Si) ion density in that region is n_i/f, and thus the emissivity will go as $\sim(n_e \times (n_i/f) \times fV) = n_e \times n_i \times V$. To first order, this is the same as for the uniform mix case and thus the correct mix mass would be inferred. There is a second order effect in that the electron density will be slightly modified since this depends on the sum of the local CH(Si) and DT ion densities; however, this is a small correction except where the CH(Si) mix fraction is very large. Further, if ablator mix were locally confined in radial space (e.g., a cooler region at the edge of the hot spot), the inferred mix mass would change, but not the radiation loss.

The error bars in the calculation represent the goodness of the weighted χ^2 fit to the five Ross filter channels. The statistical error in each of the five channels is determined separately based on the signal to noise level, background subtraction, number of images integrated over, etc., which vary between shots. Thus, while most shots produce good fits, some shots will produce worse fits with a larger χ^2 and result in larger error bars. The main uncertainty in the calculated enhancement ratio and mix fraction arises from the uncertainty in the shell attenuation. A detailed estimation of the error bars on the model itself would require 2D and 3D simulations of various shapes of the hot spot and is out of the scope of the present paper. This may be a topic of future research.

We also note that the calculation is significantly more complex when the optical depth effects are important, as in the case for resonance line emission from impurities. A major advantage of our method, which uses high energy continuum x-ray emission, is that the hot spot is optically thin and thus calculating the total emission from the hot spot volume is relatively straightforward.

IV. MIX TRENDS IN LOW-FOOT AND HIGH-FOOT DT IMPLOSIONS

The low-foot class of implosions refers to capsules that were driven with a four-shock pulseshape where the picket (initial shock) and trough (long duration low level of the laser between the first and second shocks) are at a relatively low level (picket is <20 TW). The highest neutron yield obtained for this set of shots was 8.5×10^{14}. One of the primary factors in limiting the yield is believed to have been mix.

Figure 4 plots the measured total neutron yield across the ensemble of cryogenic low-foot DT experiments against their inferred CH(Si) mix mass (which scales with the x-ray enhancement factor). The different colors represent varying peak laser powers used to drive the individual shots, and as can be seen, there is large variability in the amount of measured mix. Nonetheless, there is clearly a trend of neutron yield dropping with increasing mix.

These experimental yields were 3–20× lower than predicted by 2D post-shot simulations that incorporated delivered laser, and capsule and ice surface roughnesses.[30] Further, the scaling of DT neutron yield with ion temperature of $Y \sim T_{ion}^{2.4}$ in these experiments[11] was far more gradual than predicted by theoretical scalings ($Y \sim T_{ion}^{4.7}$).[31] However, when enhanced (preloaded) mix was included in the simulations, then similar DT yield to T_{ion} scalings be recovered, indicating that radiative cooling through mix was playing a significant role in the performance of the low-foot implosions.

Lower convergence, higher adiabat "high-foot" implosions[32–34] were predicted to improve implosion stability and offer an alternate route to higher yield-over-clean and alpha heating. The higher foot, i.e., the picket and trough, drives a stronger first shock. This results in more ablative stabilization at early time.[35,36] There is one less shock, which means less associated Richtmyer-Meshkov instability, and also increased density scale-length at late time, combined with modestly lower convergence to give less overall hydroinstability growth. In the high-foot platform, overall compression is exchanged for stability.

Direct experimental measurements using the Hydrodynamic Growth Radiography (HGR) technique[37,38] showed that unstable growth at the ablation front was reduced by ~5× in implosions driven with the high-foot pulse as compared to the low-foot, low-adiabat designs.[39,40]

Indeed, the lower instability growth rate of the high foot was corroborated by low x-ray enhancement in DT implosions, as shown in Fig. 5. The same capsule and hohlraums were used as in the low-foot campaign, but the neutron yield increased, approaching 10^{16}, most likely as a result of lower convergence, with lower instability growth, and thus with lower mix mass.

Because the high-foot implosions were stable with low levels of mix, there was latitude to thin the ablator.[41] The thinner the ablator, the less payload mass there is to accelerate, allowing for higher implosion velocities to impart more energy (via PdV work) into the nuclear fuel. However, it is a trade-off with protecting the fuel and hot spot from feedthrough of instabilities. Two ablators thinner than the nominal 195 μm thick ablator were tested: 10% and 15% thinner ablators of 175 μm and 165 μm, respectively.

Figure 6 shows the increase in neutron yield across a series of high-foot shots for a given ablator as the laser energy used to drive the implosion (and thus the implosion velocity) was increased. The abrupt vertical increase in yield at the higher laser energies for a given ablator thickness is a result of either exchanging the Au hohlraum for DU (which provides ~25 TW additional drive[42]), or an improvement in implosion symmetry, or both. Importantly, this plot also shows that at the same laser energy, the thinner ablators could attain higher neutron yield due to their increased velocity.

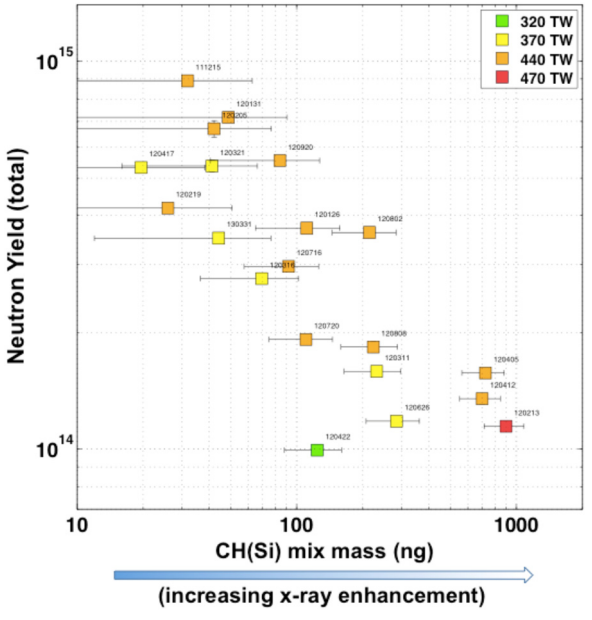

FIG. 4. DT neutron yield versus inferred mix mass for the layered low-foot implosions. Points are color coded by peak laser power. The 25 TW increase in effective peak power when DU hohlraums are used[29] is accounted for here.

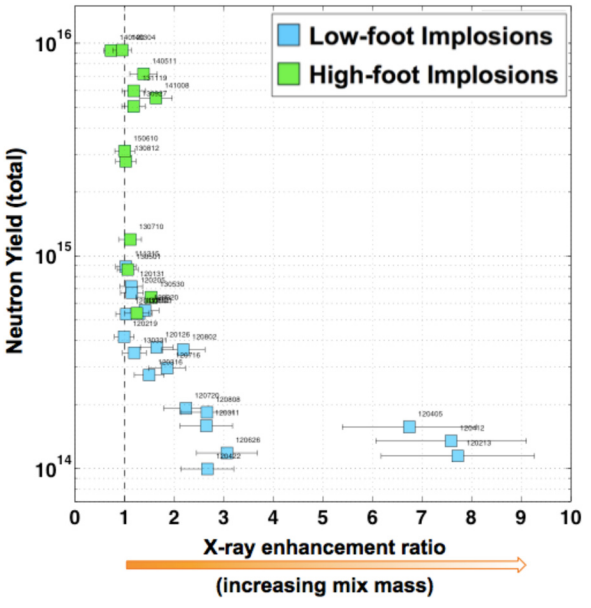

FIG. 5. DT neutron yield versus measured x-ray enhancement ratio for the layered low-foot (blue) and high-foot (green) implosions.

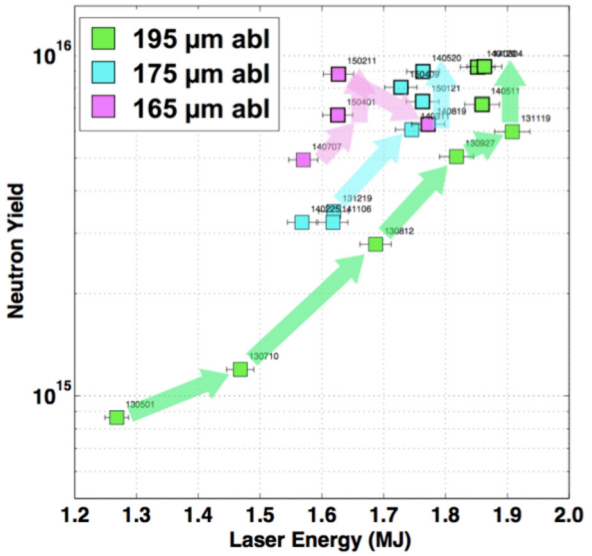

FIG. 6. Achieved neutron yields versus laser energy to drive the implosion using a high-foot pulseshape for varying ablator thicknesses (195 μm, green; 175 μm, cyan; and 165 μm, magenta). Points bounded by thicker solid lines used a DU hohlraum.

However, performance of the 15% thinner ablator implosion did roll over when pushed to 1.77 MJ. An investigation of the x-ray enhancement factor (Fig. 7) shows that mix remained low across all ablator thicknesses of the high-foot implosions, so the reason for the performance cliff was not mix becoming a major factor again. The leading hypothesis for the observed decreased performance of this shot (N140819) is actually that ablator confinement was lost due to thin spots in the shell.[43–45] This is corroborated by a near-zero ablator optical depth on this shot as inferred from the Edge Filters (Fig. 8) and a very low carbon ρr from the GRH diagnostic which measured the γ-ray signal

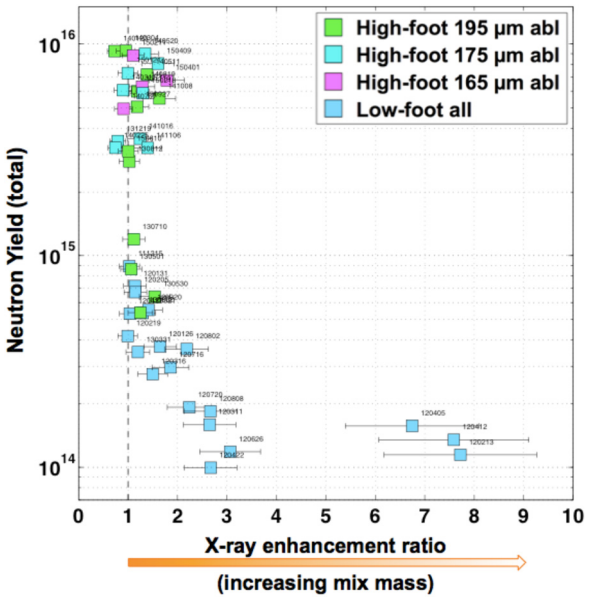

FIG. 7. Adding the 175 μm and 165 μm thick ablator experiments to the plot of Fig. 5 shows that no significant increase in mix was seen with the thinner ablators over the nominal 195 μm when driven with the high-foot pulseshape.

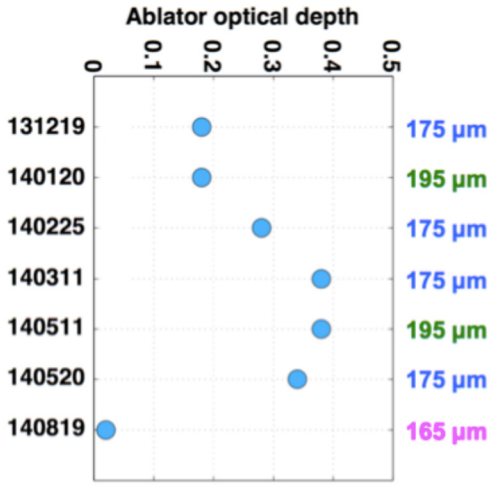

FIG. 8. Optical depth of the shell at 10.85 keV as inferred from the Ross filters along the north pole line-of-sight (spatially integrated over the entire emitting region). The capsules with 195 μm or 175 μm ablator thickness showed appreciable shell thickness. However, the thinnest ablator of 165 μm showed nearly zero optical depth.

from inelastic neutron scattering of ^{12}C in the ablator material.[46] A highly modulated 3D shell with areas of low areal density would provide little inertial confinement and allow a path for hot spot energy and mass loss (i.e., hot spot decompression).

Given the increased stability of the high-foot implosions, velocities of >380 km/s were demonstrated with little indication of hydrodynamic mix (see Fig. 9), a significant achievement over the slower 300–340 km/s low-foot implosions that were yet still susceptible to mix.

Notably, as Fig. 10 shows, in comparing the yield measured across these high-foot and low-foot shots against their individual ion temperatures, it is seen that with the high-foots, a strong power scaling ($Y \sim T^{4.1}$) is recovered, more consistent with expectations from the 1D theory.

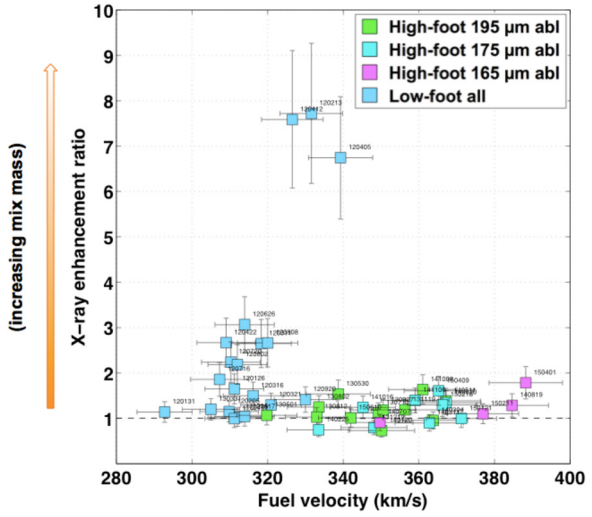

FIG. 9. X-ray enhancement versus fuel velocity. The severe levels of mix mass when the low-foot implosions were pushed limited the peak demonstrated fuel velocity to 340 km/s. The stable, low mix high-foot implosions achieved over 380 km/s.

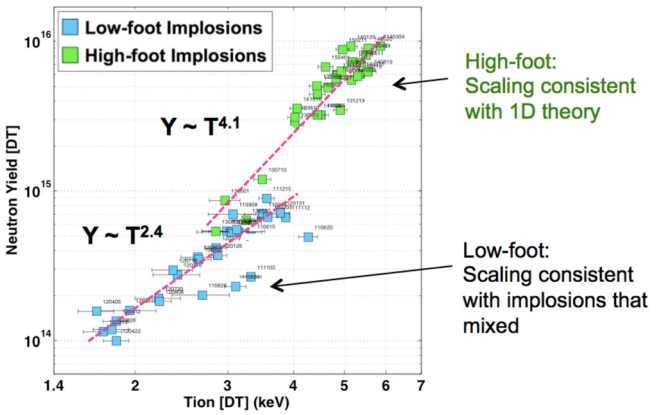

FIG. 10. The DT neutron yield to T_{ion} scaling of the high-foot implosions shows much better consistency with 1D expectations in the absence of mix. The gradual scaling of the low-foots is attributed to radiative cooling of the hot spot due to mix.

V. CONCLUSIONS

Hydrodynamic mix in ICF implosions is a critical performance limitation that must be measured, understood, and controlled. Ablator penetration into the fuel and hot spot results in increased radiation loss, cooling of the hot spot, and reduced neutron yield. By comparing the ratio of the measured x-ray continuum brightness to the neutron yield, we can quantify the level of mix. The principal source of performance variability for the low-foot implosions is attributed to mix, whereas high-foot implosions showed less susceptibility to mix and allowed velocities of >380 km/s to be demonstrated.

Whilst significant mix has not been observed in the high-foots via this 2D imaging continuum method, there is some evidence that the fill tube, capsule support tent, or imperfections in the capsule or DT ice surface are producing some mix,[47] which manifest as localized spots of emission. Future work includes isolating these features to determine the level of localized radiative cooling and the development of new diagnostics to provide higher temporal and spatial resolution to resolve and quantify these features.

ACKNOWLEDGMENTS

We wish to thank the NIF operations team. This work was performed under the auspices of the U.S. Department of Energy by Lawrence Livermore National Laboratory under Contract No. DE-AC52–07NA27344 and by General Atomics under Contract No. DE-NA0001808.

[1]G. H. Miller, E. I. Moses, and C. R. Wuest, Nucl. Fusion **44**, S228 (2004).
[2]J. Nuckolls, L. Wood, A. Thiessen, and G. B. Zimmerman, Nature **239**, 139 (1972).
[3]S. Atzeni and J. Meyer-Ter-Vehn, *The Physics of Inertial Fusion* (Oxford Science, 2004).
[4]L. Rayleigh, *Scientific Papers II* (Cambridge University Press, 1900), p. 200.
[5]G. Taylor, Proc. R. Soc. London **201**, 192 (1950).
[6]S. W. Haan, J. D. Lindl, D. A. Callahan, D. S. Clark, J. D. Salmonson, B. A. Hammel, L. J. Atherton, R. C. Cook, M. J. Edwards, S. Glenzer *et al.*, Phys. Plasmas **18**, 051001 (2011).
[7]T. Doppner, C. Thomas, L. Divol, E. Dewald, P. Celliers, D. Bradley, D. Callahan, S. Dixit, J. Harte, S. Glenn *et al.*, Phys. Rev. Lett. **108**, 135006 (2012).
[8]D. S. Clark, S. W. Haan, B. A. Hammel, J. D. Salmonson, D. A. Callahan, and R. P. J. Town, Phys. Plasmas **17**, 052703 (2010).
[9]S. P. Regan, R. Epstein, B. A. Hammel, L. J. Suter, J. Ralph, H. Scott, M. A. Barrios, D. K. Bradley, D. A. Callahan, C. Cerjan *et al.*, Phys. Plasmas **19**, 056307 (2012).
[10]S. P. Regan, R. Epstein, B. A. Hammel, L. J. Suter, H. A. Scott, M. A. Barrios, D. K. Bradley, D. A. Callahan, C. Cerjan, G. W. Collins *et al.*, Phys. Rev. Lett. **111**, 045001 (2013).
[11]T. Ma, P. K. Patel, N. Izumi, P. T. Springer, M. H. Key, L. J. Atherton, L. R. Benedetti, D. K. Bradley, D. A. Callahan, P. M. Celliers *et al.*, Phys. Rev. Lett. **111**, 085004 (2013).
[12]D. L. Bleuel, C. B. Yeamans, L. A. Bernstein, R. M. Bionta, J. A. Caggiano, D. T. Casey, G. W. Cooper, O. B. Drury, J. A. Frenje, C. A. Hagmann *et al.*, Rev. Sci. Instrum. **83**, 10D313 (2012).
[13]D. T. Casey, J. A. Frenje, M. Gatu Johnson, F. H. Seguin, C. K. Li, R. D. Petrasso, V. Y. Glebov, J. Katz, J. P. Knauer, D. D. Meyerhofer *et al.*, Rev. Sci. Instrum. **83**, 10D912 (2012).
[14]R. A. Lerche, V. Y. Glebov, M. J. Moran, J. M. McNaney, J. D. Kilkenny, M. J. Eckart, R. A. Zacharias, J. J. Haslam, T. J. Clancy, M. F. Yeoman *et al.*, Rev. Sci. Instrum. **81**, 10D319 (2010).
[15]T. Ma, N. Izumi, R. Tommasini, D. K. Bradley, P. Bell, C. J. Cerjan, S. Dixit, T. Doppner, O. Jones, J. L. Kline *et al.*, Rev. Sci. Instrum. **83**, 10E115 (2012).
[16]N. Izumi, T. Ma, M. Barrios, L. R. Benedetti, D. Callahan, C. Cerjan, J. Edwards, S. Glenn, S. Glenzer, J. Kilkenny *et al.*, Rev. Sci. Instrum. **83**, 10E121 (2012).
[17]S. F. Khan, P. M. Bell, D. K. Bradley, S. R. Burns, J. R. Celeste, L. S. Dauffy, M. J. Eckart, M. A. Gerhard, C. Hagmann, D. I. Headley *et al.*, in *SPIE Optical Engineering + Applications*, edited by P. Bell and G. P. Grim (SPIE, 2012), p. 850505.
[18]H. A. Scott and S. B. Hansen, High Energy Density Phys. **6**, 39 (2010).
[19]P. Ross, J. Opt. Soc. Am. **16**, 433 (1928).
[20]M. M. Marinak, S. W. Haan, and T. R. Dittrich, Phys. Plasmas **5**, 1125 (1998).
[21]D. H. Edgell, D. K. Bradley, E. J. Bond, S. Burns, D. A. Callahan, J. Celeste, M. J. Eckart, V. Y. Glebov, D. S. Hey, G. LaCaille *et al.*, Rev. Sci. Instrum. **83**, 10E119 (2012).
[22]A. G. MacPhee, D. H. Edgell, E. J. Bond, D. K. Bradley, C. G. Brown, S. R. Burns, J. R. Celeste, C. J. Cerjan, M. J. Eckart, V. Y. Glebov *et al.*, J. Instrum. **6**, P02009 (2011).
[23]G. P. Grim, N. Guler, F. E. Merrill, G. L. Morgan, C. R. Danly, P. L. Volegov, C. H. Wilde, D. C. Wilson, D. S. Clark, D. E. Hinkel *et al.*, Phys. Plasmas **20**, 056320 (2013).
[24]S. M. Glenn, L. R. Benedetti, D. K. Bradley, B. A. Hammel, N. Izumi, S. F. Khan, G. A. Kyrala, T. Ma, J. L. Milovich, A. E. Pak *et al.*, Rev. Sci. Instrum. **83**, 10E519 (2012).
[25]M. Gatu Johnson, J. P. Knauer, C. J. Cerjan, M. J. Eckart, G. P. Grim, E. P. Hartouni, R. Hatarik, J. D. Kilkenny, D. H. Munro, D. B. Sayre *et al.*, Phys. Rev. E **94**, 021202 (2016).
[26]L. C. Jarrott, L. R. Benedetti, H. Chen, N. Izumi, S. F. Khan, T. Ma, S. R. Nagel, O. L. Landen, A. Pak, P. K. Patel *et al.*, Rev. Sci. Instrum. **87**, 11E534 (2016).
[27]H. W. Herrmann, N. Hoffman, D. C. Wilson, W. Stoeffl, L. Dauffy, Y. H. Kim, A. McEvoy, C. S. Young, J. M. Mack, C. J. Horsfield *et al.*, Rev. Sci. Instrum. **81**, 10D333 (2010).
[28]D. S. Clark, S. W. Haan, A. W. Cook, M. J. Edwards, B. A. Hammel, J. M. Koning, and M. M. Marinak, Phys. Plasmas **18**, 082701 (2011).
[29]D. A. Callahan, N. B. Meezan, S. H. Glenzer, A. J. Mackinnon, L. R. Benedetti, D. K. Bradley, J. R. Celeste, P. M. Celliers, S. N. Dixit, T. Doppner *et al.*, Phys. Plasmas **19**, 056305 (2012).
[30]D. S. Clark, D. E. Hinkel, D. C. Eder, O. S. Jones, S. W. Haan, B. A. Hammel, M. M. Marinak, J. L. Milovich, H. F. Robey, L. J. Suter *et al.*, Phys. Plasmas **20**, 056318 (2013).
[31]R. Betti, P. Y. Chang, B. K. Spears, K. S. Anderson, J. Edwards, M. Fatenejad, J. D. Lindl, R. L. Mccrory, R. Nora, and D. Shvarts, Phys. Plasmas **17**, 058102 (2010).
[32]T. R. Dittrich, O. A. Hurricane, D. A. Callahan, E. L. Dewald, T. Doeppner, D. E. Hinkel, L. F. B. Hopkins, S. Le Pape, T. Ma, J. L. Milovich *et al.*, Phys. Rev. Lett. **112**, 055002 (2014).
[33]H. S. Park, O. A. Hurricane, D. A. Callahan, D. T. Casey, E. L. Dewald, T. R. Dittrich, T. Doppner, D. E. Hinkel, L. F. Berzak Hopkins, S. Le Pape *et al.*, Phys. Rev. Lett. **112**, 055001 (2014).
[34]O. A. Hurricane, D. A. Callahan, D. T. Casey, E. L. Dewald, T. R. Dittrich, T. Doppner, M. A. Barrios Garcia, D. E. Hinkel, L. F. Berzak Hopkins, P. Kervin *et al.*, Phys. Plasmas **21**, 056314 (2014).

[35]J. L. Peterson, D. S. Clark, L. P. Masse, and L. J. Suter, Phys. Plasmas **21**, 092710 (2014).
[36]O. L. Landen, K. L. Baker, D. S. Clark, V. N. Goncharov, B. A. Hammel, D. D. Ho, O. A. Hurricane, J. D. Lindl, E. N. Loomis, L. Masse *et al.*, J. Phys.: Conf. Ser. **717**, 012034 (2016).
[37]K. S. Raman, V. A. Smalyuk, D. T. Casey, S. W. Haan, D. E. Hoover, O. A. Hurricane, J. J. Kroll, A. Nikroo, J. L. Peterson, B. A. Remington *et al.*, Phys. Plasmas **21**, 072710 (2014).
[38]V. A. Smalyuk, D. T. Casey, D. S. Clark, M. J. Edwards, S. W. Haan, A. Hamza, D. E. Hoover, W. W. Hsing, O. Hurricane, J. D. Kilkenny *et al.*, Phys. Rev. Lett. **112**, 185003 (2014).
[39]D. T. Casey, V. A. Smalyuk, K. S. Raman, J. L. Peterson, L. Berzak Hopkins, D. A. Callahan, D. S. Clark, E. L. Dewald, T. R. Dittrich, S. W. Haan *et al.*, Phys. Rev. E **90**, 011102 (2014).
[40]J. L. Peterson, D. T. Casey, O. A. Hurricane, K. S. Raman, H. F. Robey, and V. A. Smalyuk, Phys. Plasmas **22**, 056309 (2015).
[41]T. Ma, O. A. Hurricane, D. A. Callahan, M. A. Barrios, D. T. Casey, E. L. Dewald, T. R. Dittrich, T. Doppner, S. W. Haan, D. E. Hinkel *et al.*, Phys. Rev. Lett. **114**, 145004 (2015).
[42]T. Doppner, D. A. Callahan, O. A. Hurricane, D. E. Hinkel, T. Ma, H. S. Park, L. F. Berzak Hopkins, D. T. Casey, P. Celliers, E. L. Dewald *et al.*, Phys. Rev. Lett. **115**, 055001 (2015).
[43]O. A. Hurricane, D. A. Callahan, D. T. Casey, E. L. Dewald, T. R. Dittrich, T. Doppner, S. Haan, D. E. Hinkel, L. F. Berzak Hopkins, O. Jones *et al.*, Nat. Phys. **12**, 800 (2016).
[44]D. S. Clark, C. R. Weber, J. L. Milovich, J. D. Salmonson, A. L. Kritcher, S. W. Haan, B. A. Hammel, D. E. Hinkel, O. A. Hurricane, O. S. Jones *et al.*, Phys. Plasmas **23**, 056302 (2016).
[45]D. S. Clark, M. M. Marinak, C. R. Weber, D. C. Eder, S. W. Haan, B. A. Hammel, D. E. Hinkel, O. S. Jones, J. L. Milovich, P. K. Patel *et al.*, Phys. Plasmas **22**, 022703 (2015).
[46]D. A. Callahan, O. A. Hurricane, D. E. Hinkel, T. Doppner, T. Ma, H. S. Park, M. A. Barrios Garcia, L. F. Berzak Hopkins, D. T. Casey, C. J. Cerjan *et al.*, Phys. Plasmas **22**, 056314 (2015).
[47]N. B. Meezan, M. J. Edwards, O. A. Hurricane, P. K. Patel, D. A. Callahan, W. W. Hsing, R. P. J. Town, F. Albert, P. A. Amendt, L. F. B. Hopkins *et al.*, Plasma Phys. Controlled Fusion **59**, 014021 (2016).
[48]P. T. Springer *et al.*, EPJ Web of Conference **59**, 04001 (2013).